Applied Nanoscience (2023) 13:4455–4469
https://doi.org/10.1007/s13204-022-02714-0

ORIGINAL ARTICLE

Impact of pulping routes of rice straw on cellulose nanoarchitectonics and their behavior toward Indigo dye

Altaf H. Basta[1] · **Vivian F. Lotfy**[1]

Received: 7 September 2022 / Accepted: 4 November 2022 / Published online: 30 November 2022

Abstract

This work deals with emphasizing the relation between particle dimension distribution of nanocellulose (PDD) particles with its efficiency as stabilizing/adsorbent agent of Indigo dye. In this respect, different pulping reagents were used in preparation of Rice straw pulps as precursors for nanocelluloses using acid hydrolysis and oxidizing agents [($KMnO_4$ and $NH_4)_2S_2O_8$] methods. The PDD was estimated by indirect method through processing the TEM images using the software ImageJ. The resulting nanocelluloses were also characterized by X-ray diffraction (XRD) and Fourier-transform infrared spectra (FTIR) together with sulfate ester and carboxyl contents. The data showed the effective role of pulping reagent on PDD. The cellulose nanocrystals (CNCs) from NaOH-AQ pulp, with the longest crystal length (204.4 ± 107.8 nm) and the lowest diameter (6.7 ± 2.3 nm), exhibited most stabilized suspension of dye; however, the highest adsorption capacity was accompanied the oxidized nanocellulose (Ox-NC) from neutral RS pulp with lowest PDD (4.98 ± 1.6 and 90.5 ± 3.14), together with highest COO content (476.46 µmol/g).

Keywords Rice straw-based nanocellulose · Sulfate ester-containing nanocellulose · Carboxyl-containing nanocellulose · Particle dimension distribution · Stability/absorption indigo dye

Abbreviations

PDD	Particle dimension distribution
CNCs	Cellulose nanocrystals
NCs	Nanocelluloses
AQ	Anthraquinone
BH	Sodium borohydride
COO-NCs	Carboxylated nanocelluloses
COO-K-NCs	Carboxylated nanocelluloses by $KMnO_4$ reagent:
COO-APS-NCs	Carboxylated nanocelluloses by ammonium persulphate reagent:
K-ONCs	Oxidized nanocelluloses by $KMnO_4$ reagent:
APS-ONCs	Oxidized nanocelluloses by ammonium persulphate reagent:
NIH	National Institutes of Health
PCS	Photon correlation spectroscopy
BET	Surface area analysis
TEM	Transmission electron microscope
XRD	X-ray diffraction
FTIR	Fourier-transform infrared spectroscopy
SAA	Surface-active agent

Introduction

Nanomaterials are materials with particle size dimensions in the nanoscale (< 100 nm). The production of nanocelluloses is considered to be an advanced topic in the scientific and industrial societies, due to its biodegradability and availability. This type of nanomaterials leads to developing biopolymers and other composites, via improving their mechanical properties and increasing the field of applications (e.g., medical, optical, water purification, Flexible energy and electronic devices (Rusmirovic et al. 2017; Han et al. 2019; Lotfy and Basta 2020; Basta et al. 2017a, b, 2020; Basta and Lotfy 2021; Basta et al. 2021, 2022; Shu and Tang 2020; Yu et al. 2022a, b; Zeng et al. 2020a, b; Alavijeh et al. 2021; Alruwashid et al. 2021; Danish et al. 2021; Kwon et al. 2022; Vaikundam et al. 2022).

The extraction of nanocelluloses is carried out by mechanical treatment, chemical reagents acid hydrolysis and TEMPO-mediated or ammonium persulfate oxidation

✉ Altaf H. Basta
altaf_basta@yahoo.com; altaf_halim@yahoo.com

[1] Cellulose and Paper Department, National Research Centre, Dokki, Giza 12622, Egypt

(Khatoon et al. 2012; Maschero et al. 2016; Filipova et al. 2018; Arai et al. 2018; Myja et al. 2018; Deckers et al. 2019), and enzymatic hydrolysis (Zhu et al. 2011; Ribeiro et al. 2019). The valorization of undesirable non-wood fibers as precursors for various products, e.g., activated carbon, carbon nanotubes, cellulose derivatives functional paper, and wood products, hydrogels for agricultural purposes, and nanocelluloses (Lavanya et al. 2011; Thakur et al. 2013; El-Saied et al. 2016; Lotfy et al. 2018; Basta et al. 2011; 2017a, 2021; Ho et al. 2021; Mateo et al. 2021) is a beneficial approach to reduce the pollution which results from traditional methods for disposing it by burning.

When the particle size plays a profound effect on properties of nanomaterials, therefore, the particle size and its distribution are essential examined. There are many techniques to estimate the particle size and particle size distribution for analyzing the dry powders and dispersed powder in suspension. These techniques are photon correlation spectroscopy (PCS), surface area analysis (BET), x-ray diffraction peak broadening analysis and transmission electron microscopy (TEM) (Krishtop et al. 2012; Arvaniti et al. 2015; Caputo et al. 2021).

In this present work, we examined the particle size distribution of three types of nanocelluloses (NCs), prepared from Rice straw pulps. The pulp precursors of NCs were prepared from pulping with different pulping agents. These pulps were separately subjected to acid hydrolysis or ammonium persulphate and potassium permanganate to synthesized cellulose nanocrystal and oxidized cellulose. The effective role of pulping reagents and methods of converting pulps to nanocellulose on particle size distribution XRD, FTIR, TGA of produced NCs, and further effect on adsorption/color stability of indigo dye were assessed.

Materials and methods

Preparation of nanocelluloses (NCs)

Bleached rice straw pulps as precursors for nanocelluloses were prepared from different pulping reagents, namely: NaOH without or with anthraquinone (AQ) and sodium borohydride (BH) additives, as well as KOH–NH_4OH, Na_2SO_3–Na_2CO_3, Na_2SO_3 and AcOH. The detailed processes and chemical constituents of pulps were included in the supplementary materials.

For preparation of Cellulose nanocrystals (CNCs), the nanocelluloses from the foregoing precursors were subjected to hydrolysis sulfuric acid (55 wt%; 8.75 ml of sulfuric acid solution per gram of pulp) at 45 ℃ for 30 min with vigorous stirring. The cellulose suspension was then diluted, centrifuged, washed, and dialyzed against distilled water until the exterior water reached neutrality before further use, and finally the resulting suspension was sonicated using probe sonicator (Sonics Vibra cell) to correctly disperse suspended nanocrystals and then freeze dried. The net yield of nanocellulose was assessed by the following in addition to calculate the yield. The percentages of S and O–SO_3 H of the synthesized CNC samples were determined via conductometric titrations (Zhou et al. 2018).

The CNCs from pulp samples Alk-RS pulp, Alk-AQ-RS pulp, Alk-BH-RS pulp, Alk-AQ-BH-RS pulp, M-Alk-AQ-BH-RS pulp, Pot-Amm-RS- pulp, Neut-RS pulp, Sulf.-RS pulp and Orgsolv-RS pulp samples were denoted as CNCs(1) to CNCs(9).

While the COO-containing nanocelluloses were prepared by potassium permanganate or ammonium persulfate reagents. In the former method: 5 g of different pulps were dispersed in 200 ml deionized acidic water (1 wt.% sulfuric acid); 10 g $KMnO_4$ and 5 g oxalic acid was added to the flask successively and reacted at 50 °C for 6 h with vigorous stirring. The reaction was stopped by adding hydrogen peroxide. Suitable amount of EDTA was added to remove the excess permanganate followed by washing repeatedly with deionized water until the supernatant turned turbid. Finally, the COO–K–NCs suspensions from pulp precursors (1–9) were dialyzed to remove acid and soluble carbohydrates and reach neutrality.

The oxidation with ammonium persulfate was achieved by the method reported in Reference (Filipova et al. 2018), but with minor modification. The oxidized nanocelluloses with different carbonyl contents were prepared, 5 g (dry weight) were soaked in distilled water (200ml), and then the suspension was heated to 70 °C in a water bath. Afterwards, APS (purity, 98%; 47 g), was added to the suspension. The mixture was then heated at 70 °C for 6 h with continuous stirring. The reaction was stopped by cooling the mixture in an ice bath, and then oxidized cellulose was filtered using a centrifuge and washed until it reached the pH of distilled water. The carboxyl group contents are obtained from the resulting conductivity curves (Jiang et al. 2013).

The COO–NCs from the foregoing RS samples oxidized by $KMnO_4$ reagent were coded from K-ONCs (1) to K-ONCs (9); while on using APS were coded from APS-ONCs (1) to APS-ONCs (9).

Characterization of nanocelluloses

Particle dimension distribution

The particle dimension distribution in our study was estimated by indirect method through processing the TEM images using the software ImageJ. ImageJ developed at the National Institutes of Health (NIH), USA is a Java-based

Table 1 Sulfate ester and carboxyl contents of CNCs and COO-CNCs from different RS-pulp precursors

Code of nanocellulose (pulp precursor)	SO_3H µmol/Kg Nannocelluloses CNCs Using H_2SO_4	COO content µmol/g	
		Nannocelluloses COO-K-NCs using $KMnO_4$ reagent	Nannocelluloses COO-APS-NCs Using APS reagent
1 (Alk-RS pulp)	6.9E + 04	192.20	239.97
2 (Al-AQ-RS pulp)	6.4E + 04	267.11	266.73
3(Alk-BH-RS pulp)	3.1E + 04	226.05	97.53
4 (Alk-AQ-BH-RS pulp)	5.9E + 04	160.69	207.84
5 (M- Alk-AQ-BH-RS pulp)	4.9E + 04	252.46	257.49
6 (Pot-Amm-RS pulp)	5.1E + 04	332.86	156.21
7 (Neutr-RS pulp)	4.7E + 04	476.44	144.91
8 (Sulf-RS pulp)	2.6E + 04	251.91	147.94
9 (Organosolv-RS pulp)	2.3E + 04	351.68	331.97

public domain image processing and analysis program, which is freely available and open-source application to suit the specific requirements of many microscopic images (Mazzoli and Favoni 2012; Kusdianto et al. 2019). The rod like-shape particles can be described using multiple length and diameter measures (horizontal and vertical projections) that are collected for determination of particle dimension distributions.

The TEM test was carried out using a JEOL (JEM-1230 FX, Japan) microscope operating at 200 kV. Few drops of diluted aqueous sonicated suspensions were deposited on copper-coated carbon grids with 200 mesh size, allowed to dry then the sample stained with 1% phosphotungstic acid.

XRD Test

The XRD patterns of nanocellulose samples were obtained with an X-ray diffractometer (EMPYREAN, Japan) using Cu-Kα radiation to determine the degree of crystallinity. The relative intensities were recorded within the range of 100–1500 at a scanning rate of 50 min^{-1} The diffraction patterns were recorded with scanning speed ranging from 4 to 60° on a 2θ scale. XRD data were analyzed using the TEAM® software. The degree of crystallinity can be determined from the following equation (Doumeng et al. 2021):

$$\text{Crystallinity}(\%) = \frac{\text{Area under crystalline peaks}}{\text{Total area under all peaks}} \times 100\%$$

$$x_c = \frac{A_c}{A_c + A_\alpha} \times 100$$

where, $x_{c:}$ the degree of crystallinity, $A_{c:\,the}$ area of crystalline peaks of diffraction and A_α: the area of amorphous peaks of diffraction.

While the crystallite size (t) was calculated by the Scherrer equation (Scherrer 1918).

$$T = \frac{K\lambda}{\beta \cos\theta}$$

where, T is the mean size of the ordered (crystalline) domains, which may be smaller or equal to the grain size, which may be smaller or equal to the particle size, K is a dimensionless shape factor, with a value close to unity. λ is the X-ray wavelength; β is the line broadening at half the maximum intensity, and θ is the Bragg angle.

Infrared spectra (FTIR)

This test was carried out to estimate the function groups of examined samples, according to Reference. The spectra were recorded in the region 4000 to 400 cm^{-1}, using JASCO4600-FT/IR.

Assessment of nanocelluloses against Indigo dye

The effective role of investigated nanocelluloses toward stability/adsorption of indigo dye was assessed via pH and time factors, by spectroscopic technique using UV–Vis Single Beam spectrophotometer (UV1720, USA). In this test 0.1 g of indigo dye was dispersed in 100 ml of nanocellulose samples that contained 2–2.5% dry weight sample (5% of indigo *w*/*w*, based on the dry weight of CNC). During the sample string, the pH of the mixture was adjusted to different values (1.1, 2.5, 5.3, 7.5 and 11.4) using sodium hydroxide and hydrochloric acid solutions. The absorption spectrum was measured of the obtained suspension at interval times 0, 2, 4, 24 and 29 h. Parallel test was carried out on indigo in absence of nanocelluloses. Standard curve of

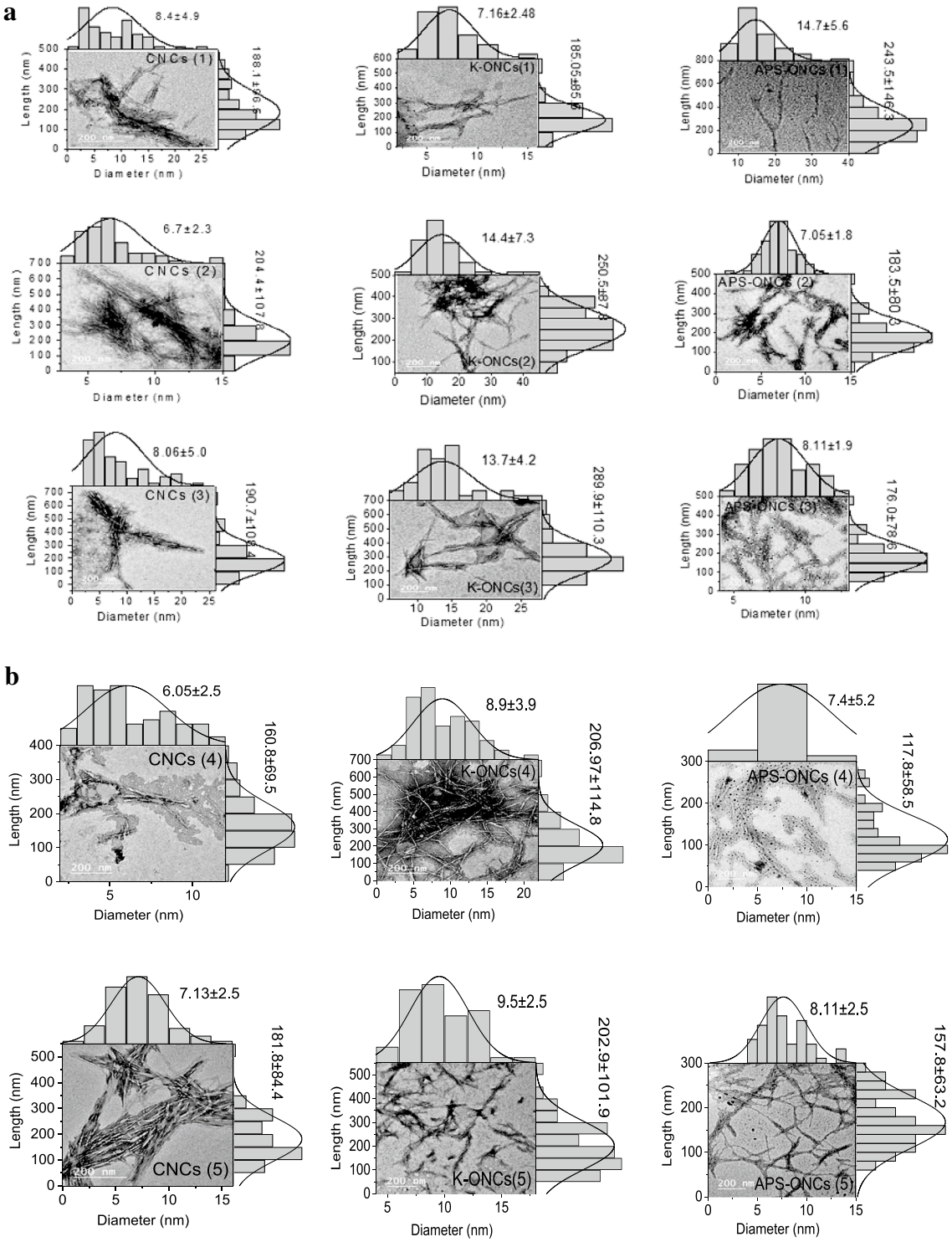

Fig. 1 **a** TEM images and PSD of nanocelluloses (1–3) from acid hydrolysis (CNCs), permanganate oxidation (K-ONCs) and APS oxidation (APS-ONCs). **b** TEM images and PSD of nanocelluloses (4–5) from acid hydrolysis (CNCs), permanganate oxidation (K-ONCs) and APS oxidation (APS-ONCs). **c** TEM images and PSD of nanocelluloses (6,7) from acid hydrolysis (CNCs), permanganate oxidation (K-ONCs) and APS oxidation (APS-ONCs). **d** TEM images and PSD of nanocelluloses (6–9) from acid hydrolysis (CNCs), permanganate oxidation (K-ONCs) and APS oxidation (APS-ONCs)

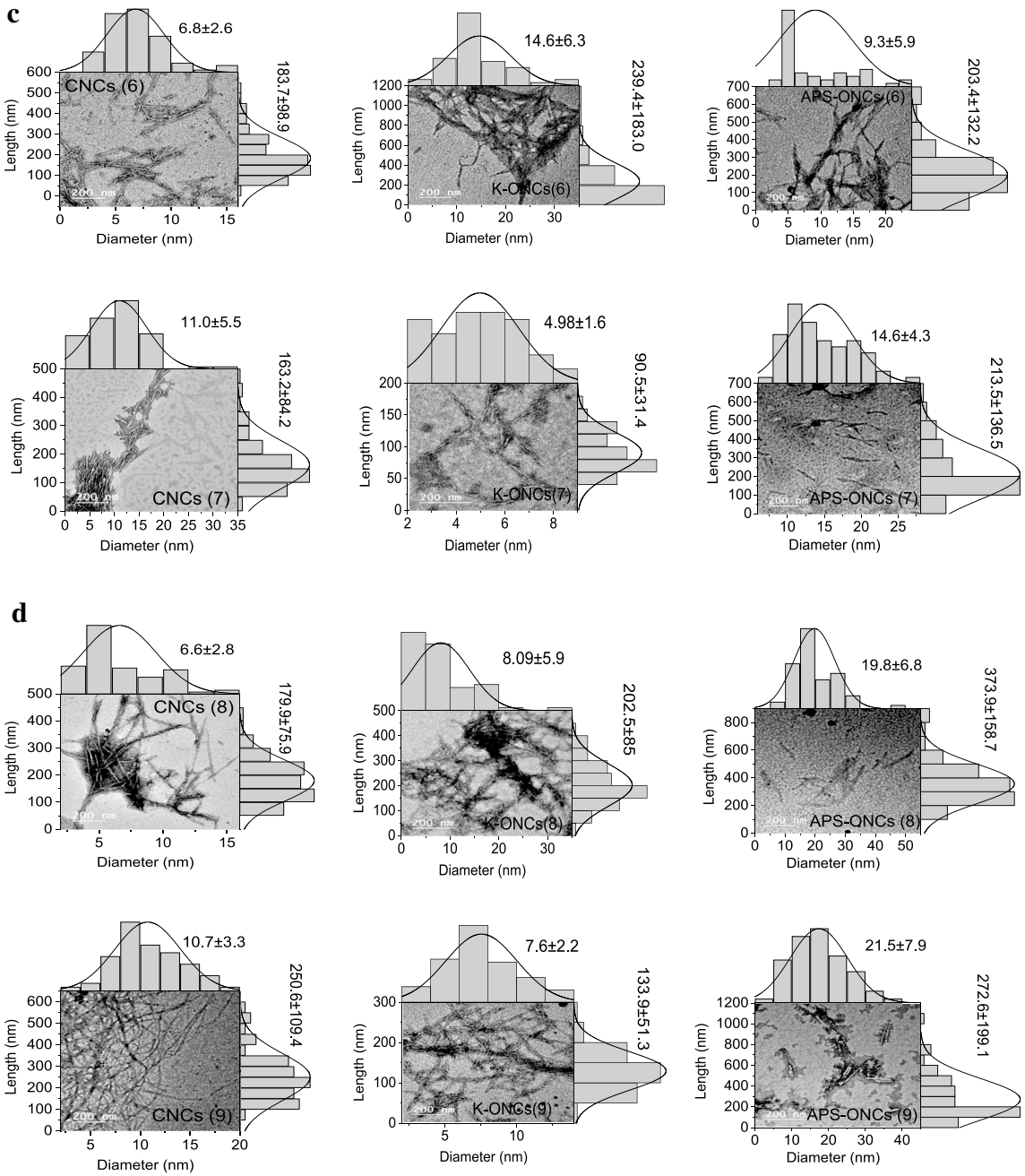

Fig. 1 (continued)

indigo was established to specify the efficiency of nanocellulose to adsorb the indigo at 704 nm (Yu et al. 2018). For the effect of Egyptol PLM (kindly supplied from Starch and Detergent Company, Alexandria, Egypt), as surface-active agent (SAA) on the stability of nanocellulose samples (3.5% of SAA *w*/*w*, based on the dry weight of CNC) it was added to Indigo-NC system followed by 2 min ultrasonics for dispersing the SAA.

Results and discussion

Characterization of nanocelluloses

Functional group contents

Table 1 illustrates the Sulfate ester contents of prepared CNCs and carboxyl contents of OCNCs, using potassium

Table 2 PSD and XRD characterization of nanocellulose samples (1–9)

Code NCs	CNCs				COO-K-NCs				COO-APS-NCs			
	PDD		XRD characterization		PDD		XRD characterization		PDD		XRD characterization	
	Diameter, nm	Length, nm	Crystallite size at $\theta = 22.5$, nm	Degree of crystallinity, %	Diameter, nm	Length, nm	Crystallite size, at $\theta = 22.5$, nm	Degree of crystallinity, %	Diameter, nm	Length, nm	Crystallite size $\theta = 22.5$, nm	Degree of crystallinity, %
Cell-RS	–	–	2.92	57.42	–	–	2.92	57.42	–	–	2.92	57.42
1	8.4 ± 4.9	188.1 ± 96.5	2.82	62.76	7.16 ± 2.48	185.05 ± 85.6	4.23	50.62	14.7 ± 5.6	243.5 ± 146.3	3.39	44.63
2	6.7 ± 2.3	204.4 ± 107.8	2.82	61.24	14.4 ± 7.3	250.5 ± 87.8	4.01	57.44	7.05 ± 1.8	183.5 ± 80.3	3.38	51.64
3	8.06 ± 5.0	190.7 ± 108.4	3.26	73.59	13.7 ± 4.2	289.9 ± 110.3	4.97	68.9	8.11 ± 1.9	176.0 ± 78.6	2.82	52.41
4	6.05 ± 2.5	160.8 ± 69.5	3.69	59.66	8.9 ± 3.9	206.7 ± 114.8	8.9	58.85	7.4 ± 5.2	117.8 ± 58.5	3.14	70.75
5	7.13 ± 2.5	181.8 ± 84.4	3.69	58.92	9.5 ± 2.5	202.9 ± 101.9	4.03	62.38	8.11 ± 2.5	157.2 ± 63.2	3.84	57.38
6	6.8 ± 2.6	183.7 ± 98.9	2.73	54.8	14.6 ± 6.3	239.4 ± 183.0	9.39	69.58	9.3 ± 5.9	203.4 ± 132.2	3.38	58.71
7	11.0 ± 5.5	163.2 ± 84.2	2.82	57.62	4.98 ± 1.6	90.5 ± 3.14	5.29	41.98	14.6 ± 4.3	213.5 ± 136.5	3.13	63.35
8	6.6 ± 2.8	179.9 ± 75.9	6.06	50.37	8.09 ± 5.9	202.5 ± 85	3.68	61.64	19.8 ± 6.8	373.9 ± 158.7	3.84	50.71
9	10.7 ± 3.3	250.6 ± 109.4	2.82	57.13	7.6 ± 2.2	133.9 ± 51.3	3.92	60.34	21.5 ± 7.9	272.6 ± 199.1	2.82	46.98

permanganate and ammonium persulphate reagents, from different RS-pulp precursors.

With regard to the data of sulfur content which indicates sulfate ester (–O–SO_3H) included the CNCs due to acid hydrolysis by H_2SO_4, it is clear that the content is affected by the type of pulp precursor. The content of sulfate ester ranged from 2.3 to 6.9E + 04 µmol/kg nanocellulose. Alkaline pulping both by soda and potassium hydroxide-Ammonium hydroxide provided CNC with relatively higher ester contents [CNCs (1); 6.9E + 04 µmol/kg and CNCs (6): 5.9E + 04 µmol/kg] than neutral sulfite and acidic agents (4.9, 5.1 and 4.7E + 04 µmol/kg, respectively). With regard to the effect of additives to soda pulping, it is noticed that anthraquinone (Na_2O-AQ pulp) is preferred than sodium borohydride both individually or with anthraquinone, where it produced CNC (2) with 6.4E + 04 µmol/kg ester content; while those produced from Na_2O–BH, Na_2O–AQ-BH-Pulp and M-Na_2O-AQ-BH Pulps [CNCs (3–6)] have sulfate ester 3.1, 2.6 and 2.3E + 04 µmol/kg, respectively.

Regarding the data of carboxylic contents of nanocelluloses (ONCs) which were related to the oxidative behavior of $KMnO_4$ and APS and estimated from using conductometric titration method declared that the carboxyl content was dramatically affected by the pulping reagent of RS. In most samples the content of COO groups of ONCs obtained from $KMnO_4$ oxidation was higher than that obtained from APS oxidation. The determined permanganate carboxyl content was in the range of 161 to 476 µmol/g α-cellulose. The neutral sulfite pulping has higher carboxyl group content (Na_2SO_3–Na_2CO_3 pulp; 476 µmol/g). The content of COO groups can reach to 333 and 352 µmol/g for NCs from KOH-NH_4OH (K-NCs (7)) and AcOH pulp [(K-NCs (9)], respectively. The remaining pulps with COO content ranged from 192 to 267 µmol/g were corresponding to alkaline pulping in presence or absence of AQ and BH beside the sulfite pulping.

For NCs resulting from APS, the contents of COO groups ranged from 127 to 332 µmol/g cellulose. The highest carboxyl content was corresponding to NC of organosolv pulp (APS-NCs (9); 332 µmol/g), followed by precursors Na_2O-AQ pulp, M-Na_2O-AQ-BH pulp (− 260 µmol/g). The pulps from KOH–NH_4OH, Na_2SO_3–Na_2CO_3 and Na_2SO_3 provided NCs with COO contents 156, 145 and 148 µmol/g, respectively. The nanocellulose from Na_2O Pulp (ONC 1) is in the last sequence (COO-APS-NCs (1); 127 µmol/g). The oxidation behavior on using APS depends on a symmetrical rupture of the O–O bond of the persulfate with formation of the atomic oxygen which oxidize the active hydroxyl group of cellulose to carboxyl group (Basta et al. 2021). While the oxidation of cellulose pulp on using KMnO4 in dilute acidic medium based on reduction of the active species (MnO_4^-) to another active form (Mn3 +) which react or stabilized

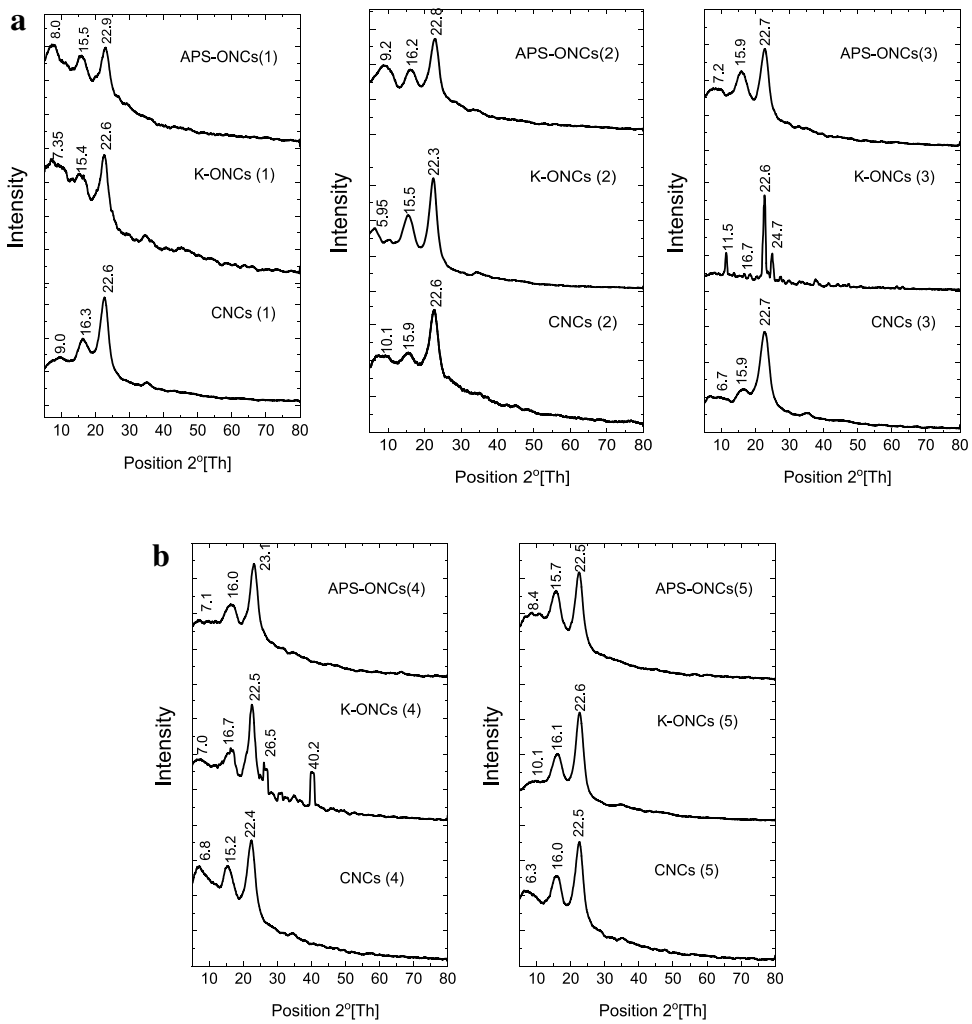

Fig. 2 **a** XRD patterns of nanocelluloses from acid hydrolysis or oxidation of Alk-RS pulp precursors without and withBH and or AQ additives of nanocellulose samples (1–3). **b** XRD patterns of nanocelluloses from acid hydrolysis or oxidation of nanocellulose samples (4–5). **c** XRD patterns of nanocelluloses from acid hydrolysis or oxidation of nanocellulose samples (6–9)

with the oxalic acid forming $[Mn(C_2O_4{}^{2-})]^+$ complex with highly oxidative activity on the amorphous regions of cellulose and converting the hydroxyl group of C2 to COO group (Zhou et al. 2018).

Particle dimension distribution

Figure 1A–D shows the TEM images of the prepared CNCs, K-NCs and APS-NCs from different RS-pulp precursors beside their calculated particle dimension distribution (PDD). The dimension of nanocelluloses was measured by ImageJ processing software (IJ 1.8) using TEM images for 50–100 measurements and gathered in Table 2. The measured diameter and length distribution of nanocelluloses resulted from the foregoing three methods having the order: CNCs < K-ONCs < APS-ONCs. The diameter of CNCs, K-ONCs and APS-ONCs ranged from 6.05 ± 2.5 to 11.0 ± 5.5, 4.98 ± 1.6 to 14.4 ± 7.3 and 7.05 ± 1.8 to 21.5 ± 7.9 nm, respectively. While the length ranges were 160.8 ± 69.5 to 250.6 ± 109.4, 90.5 ± 31.4 to 250.5 ± 87.8 and 117.8 ± 58.5 to 373.9 ± 158.7 nm for CNCs, K-ONCs and APS-ONCs respectively. This indicates the high performance of acid hydrolysis and permanganate oxidation method to get CNCs and ONCs with comparable efficiency of dimension distribution.

With regarding to the efficiency of different pulping on the dimension distribution, the results showed that the alkaline pulping with AQ and BH [CNCs (4) and APS-ONCs (4) have the lowest dimension for acid hydrolysis and APS oxidation methods with diameters 6.05 ± 2.51 and 7.4 ± 5.2 nm and length 160.8 ± 69.5 and 117.8 ± 58.5 nm, respectively (Fig. 1b). The neutral pulping with permanganate method [K-NCs (7)] was the effective pulping type to get the smallest dimension of ONCs (Fig. 1c). The less effective pulping techniques on the NCs dimension were the organsolv precursor for CNCs (9), alkaline -AQ pulp precursor for K-ONCs (2) and neutral pulp for APS-ONCs (7) as shown in Table 2. On comparing these data with literature reported CNCs from other substrates, Patel et al. 2019, reported TEM of CNCs extracted from rice husk

Fig. 2 (continued)

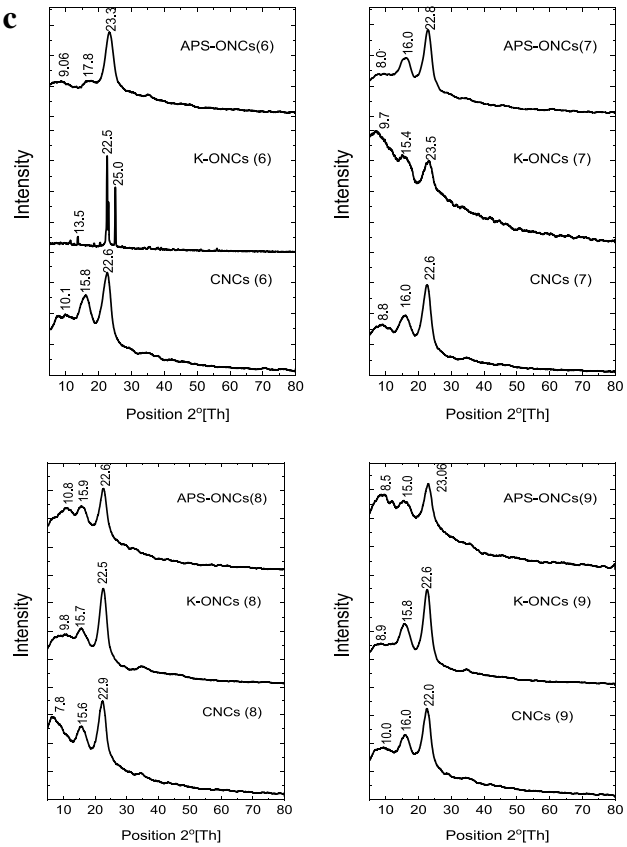

after acid hydrolysis with average length and width 128.3 and 10.5 nm calculated using image j software. Moreover, the PDD of oxidized nanocellulose obtained from wood pulp using sodium hypochlorite had average height and length of 2.7–3.2 and 173–398 nm, respectively (Matsuki et al. 2020).

XRD analysis

XRD studies of nanocelluloses from acid hydrolysis or oxidation with permanganate or APS of different RS-precursors were carried out to compare the crystalline behavior of the samples versus method and pulp precursor (Fig. 2a–c). As shown in Fig. 2, the main diffraction peaks of all nanocellulose samples are located around $2\theta = 5–10°$, 15–17° and 22–23° which are characteristic of the cellulose I family. These peaks have Miller indices (1–10), (110) and (200), respectively.

Based on the XRD results for calculating the crystallinity ratio (Table 2), the crystallinity of COO-NCs is lower compared to nanocellulose extracted using acid hydrolysis (CNCs). Typical data related to K-ONCs and APS-ONCs were noticed, where their crystallinity was in the range of 41.9–69.5% and 44.6–70.7%, respectively. While using acid hydrolysis showed crystallinity ranged from 50.3 to 73.5% with maximum value corresponding to Alk-BH pulp [CNC (3)]. The higher crystallinity ratio of ONCs were Pot-Amm-RS- pulp (69.5%) and Alk-AQ-BH-RS pulp (70.7%) for K-ONCs and APS-ONCs, respectively. The results showed deterioration of the crystallinity ratio of some nanocelluloses from acid hydrolysis or oxidation such as those produced from RS pulps, using alkaline, sulfite and neutral sulfite reagents (CNCs (1,7,8) which ranged from 41.9 to 57.3%. This decrease is probably related to some destruction of H-bonds among crystalline areas of cellulose macromolecules occurring during pulping, causing partial destruction of the crystalline zone (Ling et al. 2017). The analysis of the XRD pattern allows one to determine the average size of the crystallites using Scherrer's formula (Table 2). The average size of the crystallite of the diffraction peak located at ~ 22.5° is ranged from 2.82 to 9.39 nm.

FTIR spectral analysis

The changes in the functional groups of CNC from acid hydrolysis and COO-NCs from oxidation of different RS-pulp were studied by FTIR spectroscopy. Figure 3a–c shows the FTIR spectra of the different nanocelluloses for each RS-pulp separately. FTIR spectra of all nanocelluloses extracted with different methods are approximately identical with no

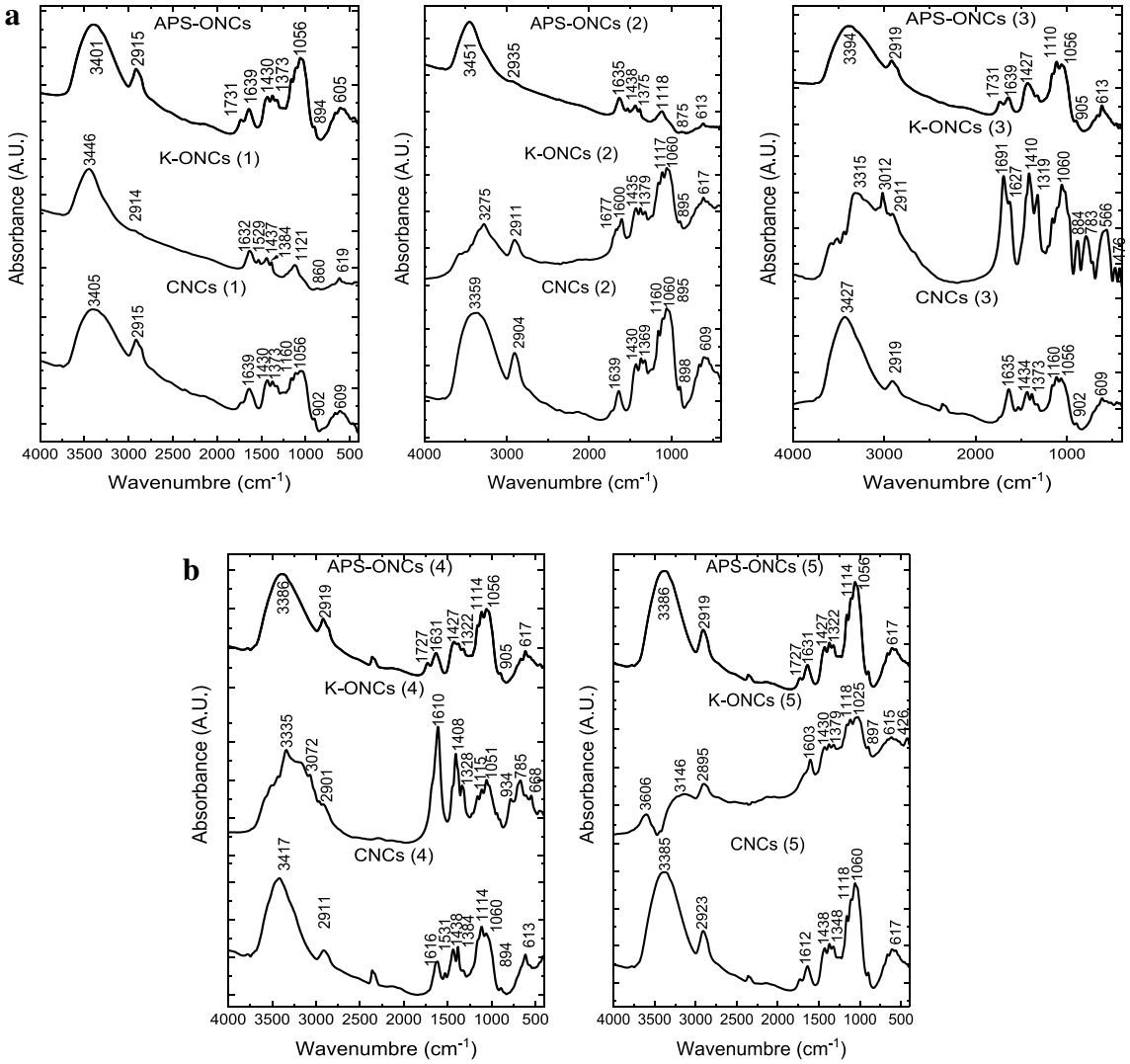

Fig. 3 **a** FTIR spectra of nanocelluloses from acid hydrolysis or oxidation of nanocellulose samples (1–3). **b** FTIR spectra of nanocelluloses from acid hydrolysis or oxidation of nanocellulose samples (4–5)

significant difference in the main characteristic peaks of cellulose, whereas OH and CH stretching vibration appeared at 3300–3400 cm^{-1}, 2900–2925 cm^{-1}. The peaks around 1600, 1400 and 1300 were assigned to OH bending of absorbed water, bending vibration of CH_2 and OCH. The C–O–C stretching vibration of the pyranose ring appeared at 1000–1100 cm^{-1} and the stretching vibration for β-(1,4)-glycosidic linkage appeared at 900 cm^{-1}. Finally, the peak around 600 cm^{-1} is assigned to the out of plane bending vibration of C–OH. All these peaks are typical of cellulose I (Oh, et al. 2005). The feature peaks at 470 cm^{-1}, 782 cm^{-1} and 1090 cm^{-1} which related to Si–O–Si stretching and bending vibration were not easily detected as they mashed with that of cellulose.

The characteristic feature of oxidized nanocelluloses (K-ONCs and APS-ONCs) in comparison with CNCs is noticed in appearing a peak around 1730 cm^{-1} together with the band peak (1610–1639 cm^{-1}), due to the carbonyl group of the carboxylic groups (Matsuki et al. 2020; Zhang et al. 2019). Matsuki et al. 2020 reported that the absorption band at ~ 1630 cm^{-1} was assigned to the asymmetric carboxylate stretching vibration. For K-ONCs, the COO groups appeared sharp with high intensity in most cases. The content of carboxyl groups of the COO-NCs as shown in Table 1 was confirmed to fall in the range of 127 to 476 µmol/g. Moreover, the peak at 2700–2800 cm^{-1} which was assigned to aldehyde and ketone was not observed of the oxidized nanocelluloses which indicates no aldehyde or ketone formed with cellulose oxidation (Jianga et al. 2017).

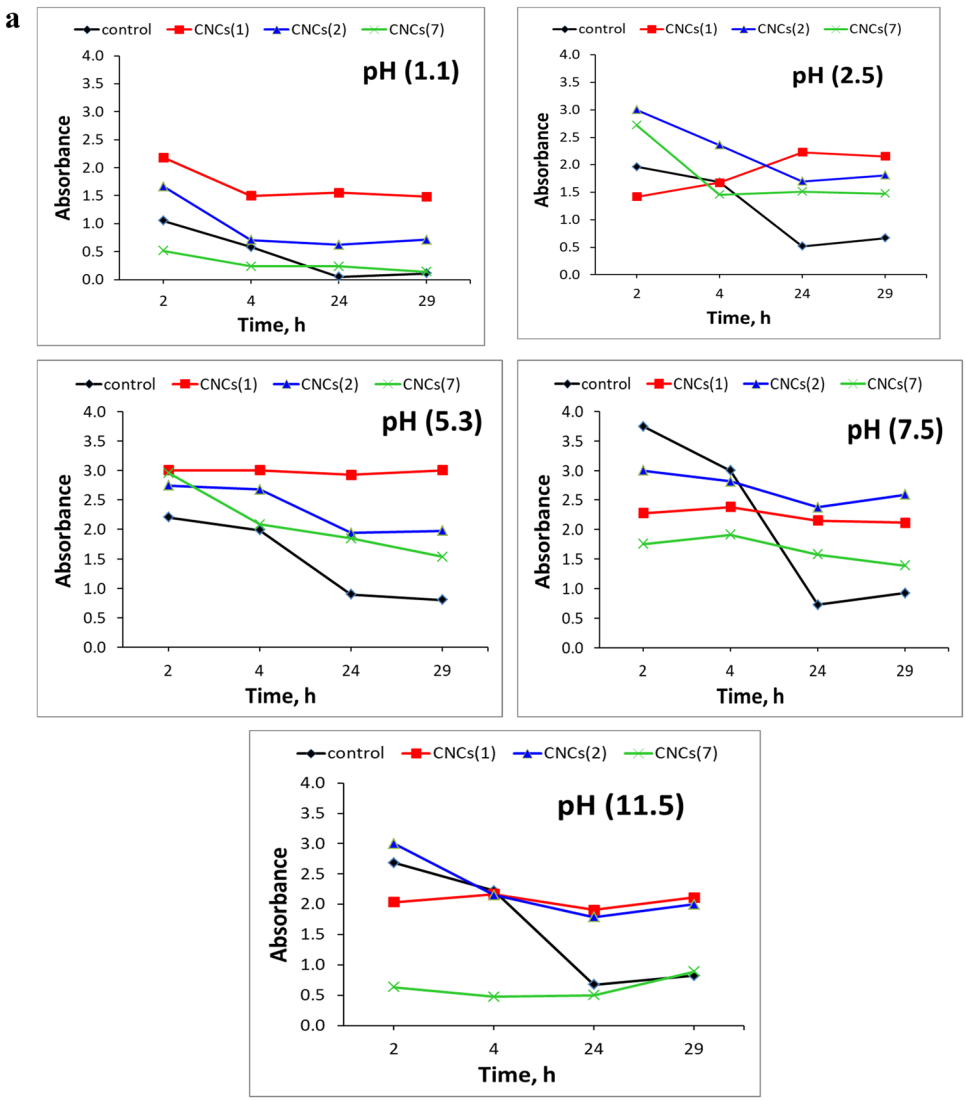

Fig. 4 **a** Changes in UV absorbance of Indigo dye loaded with CNCs versus time, at different pH's. **b** Changes in UV absorbance of Indigo dye loaded with K-ONCs versus time, at different pH's

Assessment of nanocelluloses vs color stability (indigo dispersion)/adsorption of Indigo dye

Indigo stability dispersion

Based on the foregoing data, the CNCs and K-ONCs samples, with different particle size, were candidates, for further evaluating their role toward color stability/ adsorption of indigo dye. Figures 4a, b and 5 show the stability of indigo dye in presence of nanocelluloses with time at different pH's, in comparison with control solution of indigo dye in water. As clear, the intensity absorbance at 704 nm of the control solution decreased with time regardless of the value of pH.

Figure 4a, b shows that nanocelluloses loaded indigo provided stability, the CNCs obtained from the acid hydrolysis showed higher stability as compared with those obtained from K-ONCs.

Among the acid hydrolysis nanocelluloses, the order of stability was CNCs (2) > CNCs (1) > CNCs (7) especially at the acidic PH's. In case of CNCs, the nanocelluloses prepared from Alk-AQ-RS pulp [CNCs (2)] suspension had stability over the control at acidic or slightly acidic pH media (1.1, 2.5 and 5.3) with the time interval. While the other pH media presented higher or equal stability of the indigo dye over the four hours. The Alk-RS pulp nanocellulose [CNCs (1)] showed stability over the control at only acidic pH (1.1) and the slightly acidic pH media (5.3) with all-time interval. After 4 h, the CNCs (1) suspension had higher efficiency for stabilizing the indigo dye. Finally, the stability of CNCs (7) suspension was observed only at slightly acidic pH media (5.3) and the remaining pH values the stability was observed after 24 h. The mechanism of the nanocellulose stabilizing effect is most likely related to the particle dimension distribution of nanocelluloses. The

Fig. 4 (continued)

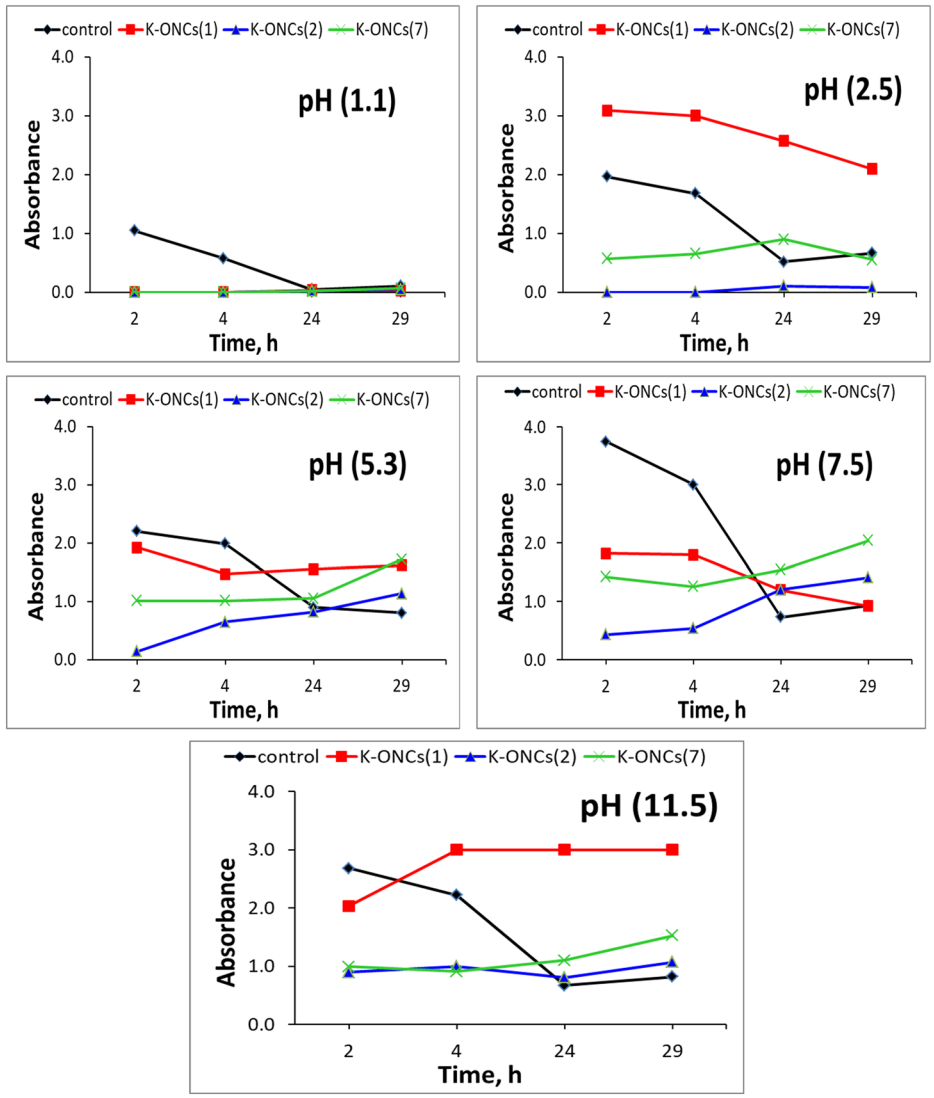

most stabilized CNCs suspension [CNCs (2)] of indigo dye had the longest crystal length (204.4 ± 107.8 nm) and the lowest diameter (6.7 ± 2.3 nm) of the candidate samples. The opposite behavior was noticed for the lowest stabilized suspension [CNCs (7)] that had the shortest crystal length (163.2 ± 84.2 nm) and relatively highest diameter 11.0 ± 5.5 nm (Table 2 and Fig. 1).

With respect to the oxidized nanocelluloses (Fig. 4b), the indigo stability in K-ONCs suspension increased with increasing pH value. As noticed, the stability was observed after 4 h for K-ONCs (1) suspension at acidic pH (2.5) and alkaline pH (11.5). After 24 h, the indigo stability was observed for K-ONCs (1) suspension at pH (2.5, 7.5 and 11.5). For the case of K-ONCs (2) and K-ONCs (7) the stability was noticed at pH from 5.3 to 11.5 and 2.5 to 11.5, respectively. In a relation with particle dimension distribution, the most stabilized oxidized nanocelluloses of the indigo were K-ONCs (1) and K-ONCs (7) which had lowest diameter crystal 7.16 ± 2.48 and 4.98 ± 1.6 nm, respectively; while the K-ONCs (2) had 14.4 ± 7.3 nm of the crystal diameter (Table 2 and Fig. 1).

The addition of Egyptol PLM (kindly supplied from Starch and Detergent Company, Alexandria, Egypt) was significantly affected as co-stabilizing agent, where the stability of the indigo dye was shown at all pH's (Fig. 5). As clear as the effective role of SAA as co-agent for CNCs stabilizing the Indigo solution both for CNCs (7) that had the lowest and high CNCs (2) indigo stabilization, individually. Whereas the addition of SAA provided higher indigo stability than the control or the samples without SAA (Fig. 4a). This feature was noticed for all the examined pH's.

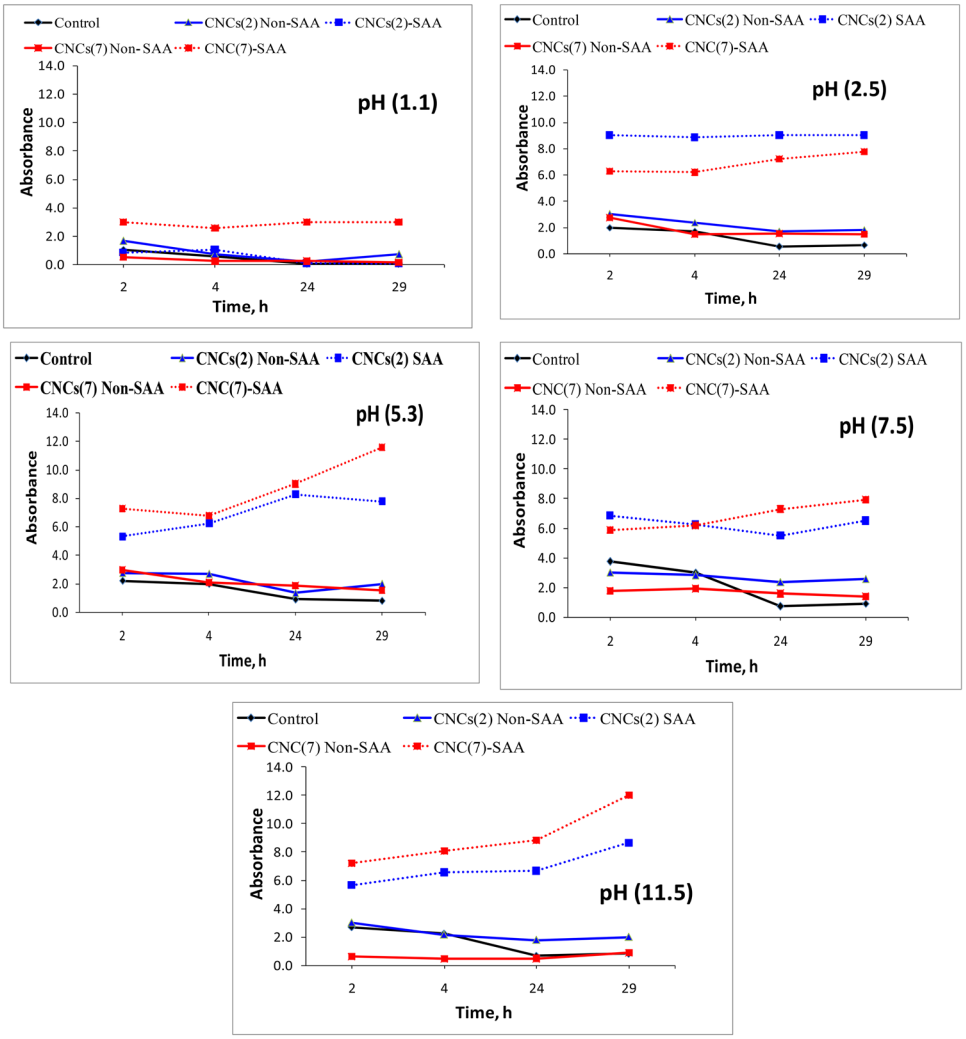

Fig. 5 Changes in UV absorbance of Indigo dye loaded with CNCs- SAA versus time, at different pH's

Indigo adsorption

The adsorption behavior of indigo dye of the nanocellulose candidate samples are shown in Fig. 6. The finding results from equilibrium adsorption of indigo dye on the nanocelluloses showed reverse behavior to the indigo stability. The nanocelluloses of K-ONCs had higher adsorption capacity than the acid hydrolysis nanocelluloses. The adsorption capacity of CNCs ranged from 7.87 to 34.6 mg/g with maximum value corresponding to CNCs (7) at lower pH (1.1). This indicates that the higher adsorption capacity of CNC was related to the lowest sulfate ester group (CNC 7: 4.7E + 4) than CNCs (1) and (2) had 6.4E + 4 and 6.9E + 4, respectively. The K-ONCs (7) indigo adsorption was in range 18.9–39.7 mg/g with maximum value observed at pH (1.1). The maximum adsorption capacity was related to K-ONCs (7), with relatively high carboxyl content of 476.46 µmol/g of the candidate samples. This indicates that the carboxyl content plays a role in promoting the indigo adsorption together with PDD.

Conclusion

In this present work the role of dimension distribution of nanocellulose particles on stability/adsorption of Indigo dye was highlighted. To emphasize this relation, different nanocelluloses were prepared by acid hydrolysis (H_2SO_4; CNCs) and oxidation methods [$KMnO_4$ (K-NCs) and APS (APS)]. The promising nanocellulose for stabilizing the Indigo dye was related to CNC from NaOH-AQ pulp precursor had the longest crystal length (204.4 ± 107.8 nm) and the lowest diameter (6.7 ± 2.3 nm); while the nanocelluloses with the diameter distribution (6.7 ± 2.3 nm) and high COO content (476.46 µmol/g), like the K-NC from RS-neutral pulp provided high adsorption capacity.

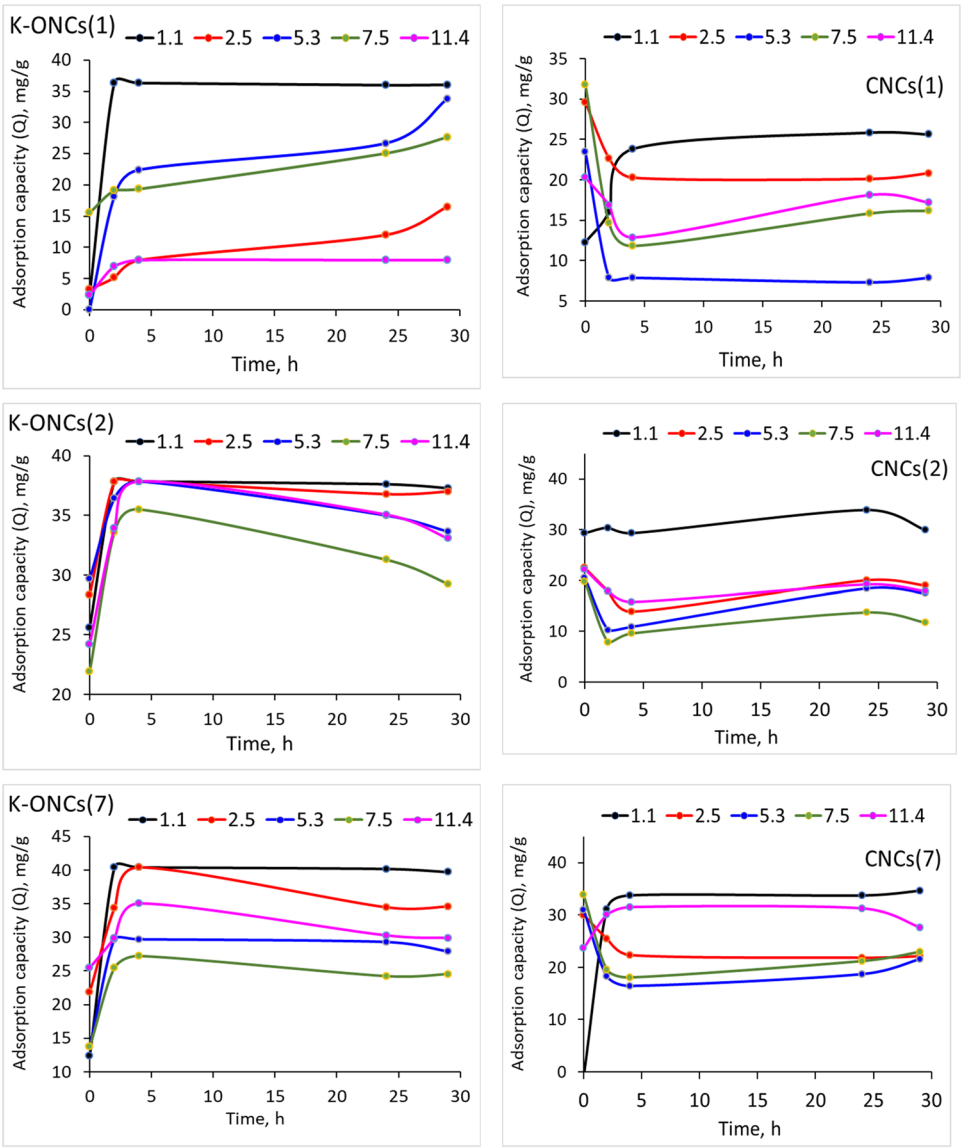

Fig. 6 Affinity of CNCs and K-ONCs to adsorb Indigo versus time at different pH's

Adding Egyptol PLM as co-agent enhanced the CNCs for stabilizing the Indigo dye in solution at all tested intervals and pH's.

Supplementary Information The online version contains supplementary material available at https://doi.org/10.1007/s13204-022-02714-0.

Acknowledgements This research work was carried out under grant Egypt-China Cooperation Program: funded by Science, Technology, and Innovation Funding Authority with Contact/Agreement No. 43068.

Funding Open access funding provided by The Science, Technology & Innovation Funding Authority (STDF) in cooperation with The Egyptian Knowledge Bank (EKB).

Declarations

Conflict of interest Authors declare that there is no conflict among the contributing author related to the financial or non-financial interests that are directly or indirectly related to the work submitted for publication.

References

Alavijeh MS, Rad I, Hatamie S (2021) Magnetic nanocomposite's mechanism of action during the hyperthermia treatment of the breast cancer. Appl Nanosci 11:2739–2746

Alruwashid FS, Dar MA, Alharthi NH, Abdo HS, Almotairy S (2021) The synthesis and characterization of graphene-based cobalt ferrite nanocomposite materials and its electrochemical properties. Appl Nanosci 11:2661–2668

Arai K, Horikawa Y, Shikata T (2018) Transport properties of commercial cellulose nanocrystals in aqueous suspension prepared from chemical pulp via sulfuric acid hydrolysis. ACS Omega 3:13944–13951

Arvaniti EC, Juenger MCG, Bernal SA, Duchesne J, Courard L, Leroy S, Provis JL, Klemm A, De Belie N (2015) Determination of particle size, surface area, and shape of supplementary cementitious materials by different techniques. Mater Struct 48(11):3687–3701

Basta AH, Girgis AS, El-Saied H, Mohamed MA (2011) Synthesis of fluorescence active pyridinedicarbonitriles and studying their application in functional. Mater Lett 65:1713–1718

Basta AH, El-Saied H, Baraka AM, Lotfy VF (2017a) Performance of carbon xerogels in the production of environmentally friendly urea formaldehyde-bagasse composites. Clean: Soil, Air, Water 45(6):1600524

Basta AH, El-Saied H, Baraka AM, Lotfy VF (2017b) Beneficial effect of new activated carbons in enhancing the performance of particle boards from UF-rice straw. Pigm Resin Technol 46(2):139–147

Basta AH, Lotfy VF, Mahmoud K, Abdelwahed NAM (2020) Synthesis and evaluation of protein-based biopolymer in production of silver nanoparticles as bioactive compound versus carbohydrates-based biopolymers. R Soc Open Sci 7(10):200928

Basta AH, Lotfy VF (2021a) Synthesis and evaluating of carbon nanoallotrope-biomacromolecule gel composites as drug delivery systems. J Appl Polym Sci 138(33):50830

Basta AH, Lotfy VF, Micky JA, Salem AM (2021b) Liquid crystal behavior of cellulose nanoparticles-ethyl cellulose composites: preparation, characterization, and rheology. J Appl Polym Sci 138(12):50067

Basta AH, Lotfy VF, Salem AM (2022) Valorization of biomass pulping waste as effective additive for enhancing the performance of films based on liquid crystal hydroxypropyl-cellulose nanocomposites. Waste Biomass Valoriz 13(4):2217–2231

Caputo F, Vogel R, Savage J, Vella G, Law A, Della Camera G, Hannon G, Peacock B, Mehn D, Ponti J, Geiss O, Aubert D, Prina-Mello A, Calzolai L (2021) Measuring particle size distribution and mass concentration of nanoplastics and microplastics: addressing some analytical challenges in the sub-micron size range. J Colloid Interface Sci 588:401–417

Danish M, Ayub H, Sandhu ZA, Shoaib A, Akram Z, Najeeb J, Naeem S (2021) Synthesis of cerium oxide/cadmium sulfide nanocomposites using inverse microemulsion methodology for photocatalytic degradation of methylene blue. Applied Nanosci 11:503–2515

Deckers C, Linden M, Löwe H (2019) Nitroxyl radical-mediated oxidation of alcohols in continuous microreactors. Chem Eng Technol 42(10):2044–2051

Doumeng M, Makhlouf L, Marsan O, Delbé K, Denape J, Chabert F (2021) A comparative study of the crystallinity of polyetheretherketone by using density, DSC, XRD, and Raman spectroscopy techniques. Polym Testing 93:106878

El-Saied H, El-Hady OA, Basta AH, El-Dewiny CY, Abo-Sedera SA (2016) Bio-chemical properties of sandy calcareous soil treated with rice straw-based hydrogels. J Saudi Soc Agric Sci 15(2):188–194

Filipova I, Fridrihsone V, Cabulis U, Berzins A (2018) Synthesis of nanofibrillated cellulose by combined ammonium persulphate treatment with ultrasound and mechanical processing. Nanomaterials 8:2–11

Han L, Cui S, Yu H, Song M, Zhang H, Huang C, Kim D, Tam KMC (2019) Self-healable conductive nanocellulose nanocomposites for biocompatible electronic skin sensor system self-healable conductive nanocellulose nanocomposites for biocompatible electronic skin sensor system. ACS Appl Mater Interfaces 11:44642–44651

Ho PH, Lotfy V, Basta A, Trens P (2021) Designing microporous activated carbons from biomass for carbon dioxide adsorption at ambient temperature. A comparison between bagasse and rice by-products. J Clean Prod 294:126260

Jiang F, Han S, Hsieh Y-L (2013) Controlled defibrillation of rice straw cellulose and self-assembly of cellulose nanofibrils into highly crystalline fibrous materials. RSC Adv 3:12366

Jianga H, Wua Y, Hana B, Zhang Y (2017) Effect of oxidation time on the properties of cellulose nanocrystals from hybrid poplar residues using the ammonium persulfate. Carbohyd Polym 174:291–298

Khatoon N, Ramezani O, Kermanian H (2012) Production of Nanocrystalline Cellulose from Sugarcane Bagasse. In: 4th International Conference Nanostructurs. p 12–14

Krishtop V, Doronin I, Okishev K (2012) Improvement of photon correlation spectroscopy method for measuring nanoparticle size by using attenuated total reflectance. Opt Express 20:25693–25699

Kusdianto K, Diastatic W, Shimada M, Qomariyah L, Winardi S (2019) Fabrication of ZnO-SiO_2 nanocomposite materials prepared by a spray pyrolysis for the photocatalytic activity under UV and sunlight irradiations. In: IOP Conference Series: Materials Science and Engineering, vol 778

Kwon S, Jamal H, Choi J-Y, Park H-H, Song J, Lee C-S (2022) Synthesis and characterization of graphene quantum dot/SiNP/carbon nanomaterial composites. Appl Nanosci. https://doi.org/10.1007/s13204-022-02676-3

Lavanya D, Kulkarni P, Dixit M, Raavi PK, Krishna LNV (2011) Source of cellulose derivatives and their applications. Int J Drug Dev Res 2:19–38

Ling Z, Chen S, Zhang X, Takabe K, Xu F (2017) Unraveling variations of crystalline cellulose induced by ionic liquid and their effects on enzymatic hydrolysis. Sci Rep 7:10230

Lotfy VF, Basta AH (2020) Optimizing the chitosan-cellulose based drug delivery system for controlling the ciprofloxacin release versus organic/inorganic crosslinker, characterization and kinetic study. Int J Biol Macromol 165:1496–1506

Lotfy VF, Fathy NA, Basta AH (2018) Novel approach for synthesizing different shapes of carbon nanotubes from rice straw residue. Environ Chem Eng J 6(5):6263–6274

Mascheroni E, Rampazzo R, Ortenzi MA, Piva G, Bonetti S, Piergiovanni L (2016) Comparison of cellulose nanocrystals obtained by sulfuric acid hydrolysis and ammonium persulfate, to be used as coating on flexible food-packaging materials. Cellulose 23:779–793

Mateo S, Peinado S, Morillas-Gutiérrez F, Dolores La Rubia M, Moya AJ (2021) Nanocellulose from agricultural wastes: products and applications—A Review. Processes 9(1594):1–22

Matsuki S, Kayano H, Takada J, Kono H, Fujisawa S, Saito T, Isogai A (2020) Nanocellulose production via one-pot formation of C2 and C3 carboxylate groups using highly concentrated NaClO aqueous solution. ACS Sustain Chem Eng 8:17800–17806

Mazzoli A, Favoni O (2012) Particle size, size distribution and morphological evaluation of airborne dust particles of diverse woods by scanning electron microscopy and image processing program. Powder Technol 225:65–71

Myja D, Loranger É, Lanouette R (2018) TEMPO Mediated oxidation optimization on thermo mechanical pulp for paper reinforcement and nanomaterial film production. BioResources 13(2):4075–4092

Oh SY, Yoo DI, Shin Y, Kim HC, Kim HY, Chung YS, Park WH, Youk JH (2005) Crystalline structure analysis of cellulose treated with sodium hydroxide and carbon dioxide by means of X-ray diffraction and FTIR spectroscopy. Carbohyd Res 340(15):2376–2391

Patel DK, Seo Y-R, Dutta SD, Lim K-T (2019) Enhanced osteogenesis of mesenchymal stem cells on electrospun cellulose nanocrystals/poly(3-caprolactone) nanofibers on graphene oxide substrates. RSC Adv 9:36040

Ribeiro RSA, Pohlmann BC, Calado V, Bojorge N, Pereira N (2019) Production of nanocellulose by enzymatic hydrolysis: trends and challenges. Eng Life Sci 19:279–291

Rusmirovic JD, Ivanovi JZ, Pavlovi VB, Raki VM, Rancic MP, Djokic V, Marinković AD (2017) Novel modified nanocellulose applicable as reinforcement in high-performance nanocomposites. Carbohyd Polym 164:4–74

Scherrer P (1918) Bestimmung der Grösse und der Inneren Struktur von Kolloidteilchen Mittels Röntgenstrahlen, Nachrichten von der Gesellschaft der Wissenschaften, Göttingen. Mathematisch-Physikalische Klasse. 2:98–100

Shu J, Tang D (2020) Recent Advances in photoelectrochemical sensing: from engineered photoactive materials to sensing devices and detection modes. Anal Chem 92:363–377

Thakur VK, Thakur MK, Gupta RK (2013) Development of functionalized cellulosic biopolymers by graft copolymerization. Int J Biol Macromol 62:44–51

Vaikundam M, Shanmugam S, Aldawood S, Arunkumar P, Santhanam A (2022) Preparation of biopolymer pectin fascinate hydroxyapatite nanocomposite for biomedical applications. Applied Nanosci. https://doi.org/10.1007/s13204-022-02578-4

Yu Y, Ma R, Yan S, Fang J (2018) Preparation of multi-layer nylon-6 nanofibrous membranes by electrospinning and hot-pressing methods for dye filtration. RSC Adv 8:12173–12178

Yu Z, Gong H, Xu J, Li Y, Xue F, Zeng Y, Liu X, Tang Di (2022a) Liposome-embedded Cu_{2-x} Ag_xS nanoparticle-mediated photothermal immunoassay for daily monitoring of cTnI protein using a portable thermal imager. Anal Chem 94:7408–7416

Yu Z, Gong H, Xu J, Li Y, Zeng Y, Liu X, Tang D (2022b) Exploiting photoelectric activities and piezoelectric properties of $NaNbO_3$ semiconductors for point-of-care immunoassay. Anal Chem 94:3418–3426

Zeng R, Wang W, Cai G, Huang Z, Tao J, Tang D, Zhu C (2020a) Single-atom platinum nanocatalyst-improved catalytic efficiency with enzyme-DNA supermolecular architectures. Nano Energy 74:104931

Zeng R, Wang W, Chen M, Wan Q, Wang C, Knopp D, Tang D (2020b) CRISPR-Cas12a-driven MXene-PEDOT: PSS piezoresistive wireless biosensor. Nano Energy 82:105711

Zhang S, Zhang F, Jin L et al (2019) Preparation of spherical nanocellulose from wastepaper by aqueous NaOH/thiourea. Cellulose 26:5177–5185

Zhou L, Li N, Shu J, Liu Y, Wang K, Cui X, Yuan Y, Ding B, Geng Y, Wang Z, Duan Y, Zhang J (2018) One-pot preparation of carboxylated cellulose nanocrystals and their liquid crystalline behaviors. ACS Sustain Chem Eng 6(9):12403–12410

Zhu JY, Sabo R, Luo X (2011) Integrated production of nano-fibrillated cellulose and cellulosic biofuel (ethanol) by enzymatic fractionation of wood fibers. Green Chem 13:1339–1344